ICARUS **119,** 130–143 (1996)
ARTICLE NO. 0006

Martian Weather Correlation Length Scales

DON BANFIELD,[1] ANTHONY D. TOIGO, AND ANDREW P. INGERSOLL

170-25 Caltech, Division of Geological and Planetary Sciences, California Institute of Technology, Pasadena, California 91125
E-mail: banfield@astrosun.tn.cornell.edu

AND

DAVID A. PAIGE

Department of Earth and Space Sciences, University of California, Los Angeles, Los Angeles, California 90024

Received May 16, 1994; revised July 27, 1995

Spring and fall equinox Viking infrared thermal mapper 15-μm channel atmospheric brightness temperature (T15) observations are used to estimate the weather correlation length scale of Mars in the pressure range 0.5–1 mbar. The results provide a better understanding of martian atmospheric dynamics, a benchmark for validating martian general circulation models (GCMs), a guide to the optimal placement of a network of landers, and information for use in data assimilation efforts for orbiters and landers. Observations of atmospheric temperature are used to compute an atmospheric mean state as a function of time-of-day, latitude, longitude, and altitude, which is then subtracted from the observations to yield weather temperature residuals. These residuals are correlated with each other to determine (1) the weather temperature correlation length scale (~1000 km) as a function of latitude and (2) the weather temperature variance (~4 K^2 global average for $L_S \sim 0°$, ~3 K^2 for $L_S \sim 180°$). Good general agreement is found in comparing the length scales to the Rossby radius of deformation and to inferences made from other data sets. The weather temperature variance results are also compared with GCM results, yielding satisfactory agreement, with some differences in the magnitudes of the variances.

1. INTRODUCTION

Mars has weather. Baroclinic waves and perhaps even frontal systems have been observed passing over the Viking Landers (e.g., Barnes 1980, Tillman *et al.* 1979). The Mariner and Viking Orbiters observed many types of clouds, which resemble what we consider weather on Earth (Kahn 1984). Local and global dust storms have been observed on Mars for roughly a century (Martin and Zurek 1993). However, although we are aware that there is weather on Mars, we know very little about it. To date, the lack of low-altitude orbiters systematically mapping the atmospheric state and the existence of only two surface stations have severely limited our knowledge of atmospheric phenomena on Mars. The simplest details of the weather are still poorly constrained by the existing analyses of the martian atmospheric data sets. For example, the length scale over which a weather system can be considered a coherent body has not been directly determined. The main focus of this work is to quantify the length scale of weather systems on Mars. For the purposes of this paper, "weather" is defined as all variations in the atmosphere (in this case we only studied temperature variations) which are not simply functions of altitude, latitude, time of day, longitude, or season. That is, traveling waves of *all sorts.*

The weather correlation length scale is important for a number of reasons. The first is simply to better understand the nature of the weather systems on Mars. The length scale and shape of weather correlations are indicative of the spatial coherence of the atmospheric variations, and perhaps the dominant lengths of waves in the atmosphere. These physical quantities of the martian atmosphere and its weather add a crucial benchmark with which to evaluate the performance and validity of existing martian GCMs. While other work has allowed the temporally averaged meridional cross sections in these models to be well compared with observations (e.g., Santee and Crisp 1992, Haberle *et al.* 1993), weather phenomena in these models have been constrained mainly by the Viking Lander observations located at just two surface points (Barnes *et al.* 1993).

Another reason for wanting to know the weather correlation length scale is for use in the assimilation of observational data into numerical models: data assimilation. With Mars Observer, it was planned to take the atmospheric

[1] Present address: CRSR, Cornell University, Ithaca, NY, 14853.

0019-1035/96 $12.00

data from the pressure modulator infrared radiometer (PMIRR) instrument which would have given continuous soundings of the temperature structure of Mars' atmosphere and assimilate them into a martian GCM (Banfield *et al.* 1995). This could be realized with future missions studying Mars' atmosphere, yielding an accurate estimate of the complete martian atmospheric state at all times during the mission. However, to properly insert data into a model, the length scale over which weather systems are correlated is needed. With an optimally designed assimilation scheme, an observation at one location will influence the state of the model over a region specified roughly by this weather correlation length scale. If this length scale is not properly specified, significant performance decreases are found in the data assimilation system's accuracy (Banfield *et al.* 1995). The technique outlined in Banfield *et al.* (1995) requires the use of a GCM to predict the weather correlation length scales. Determining this length scale from data will allow us to better understand the errors made in using a GCM as a substitute for Mars.

Seaman (1977) showed that the optimal placement of a network of landers is directly related to the weather correlation length scale. Thus, understanding the nature of this quantity, as it changes with latitude, season, and dustiness of the atmosphere, can help us intelligently decide where to place landers for future meteorological investigations of Mars, such as a meteorological network.

In this work, we determine the martian weather correlation length scale using Viking Orbiter infrared thermal mapper (IRTM) 15-μm atmospheric brightness temperature (T15) observations. However, before proceeding to that portion of the work, we present the results of some techniques used to estimate the order of magnitude of this quantity. We do this using simple theory and Viking Lander meteorological data. Then we proceed to discuss the techniques we use to extract only weather effects from the IRTM T15 data and produce the weather correlations. After presenting our results, we compare them with the simple estimates, results from the Earth, and published results from a Mars GCM and other analyses of observations.

2. FIRST ESTIMATES

2.1. Theory

Some simple estimates of the weather correlation length scale can be inferred from theory. Using quasi-geostrophic theory, we expect the weather correlation length scale to be roughly the same as the Rossby radius of deformation, the length scale at which buoyancy and rotational effects are comparable (e.g., Ghil *et al.* 1979, Krauss *et al.* 1990). The Rossby radius of deformation can be defined by $L_D = NH/f$, where N is the buoyancy frequency of the atmosphere, H is the equivalent depth, and f is the Coriolis parameter. For Mars, N is about 0.01 Hz, H is about a scale height, 11.5 km (Barnes 1984), and $f = 2\Omega \sin \phi$, yielding $L_D \sim 800 \text{ km} \times (\sin \phi)^{-1}$. Thus for mid-latitudes, where the atmospheric wave activity is probably centered, we might expect a weather correlation length scale of order 1000 km.

2.2. Viking Lander Data

There were two Viking Landers operating on the surface of Mars from September 1976 until April 1980. Viking Lander 1 continued to return data until November of 1982. Among the data returned by the landers were surface pressure, temperature, and wind observations at the two sites. Barnes (1980, 1981) and Murphy *et al.* (1990) interpreted these data as indicative of baroclinic waves propagating in the martian atmosphere. They reported frequency spectra as a function of season for the pressure, wind, and temperature data taken at the site of Viking Lander 2 (48°N, 226°W) and Viking Lander 1 (22.5°N, 48°W).

From their results, one can surmise the correlation time of martian weather, at least at the latitude and times the observations were taken. The widths of the peaks in the frequency spectra are indicative of the inverse of the correlation times of the atmospheric waves. Reading from Figs. 12, 13, and 14 in Barnes (1980), a rough number of 0.08 sol^{-1} for the full width at half-maximum is found from the spectra during fall, winter, and spring. If we assume these spectral peaks represent waves which have oscillatory and damped components of the form $e^{i\omega t - t/\tau}$, and then Fourier transform this to yield the resulting power spectral density, we find

$$P(\omega) = \frac{1/\tau}{1/\tau^2 + \omega^2}. \quad (1)$$

Equating the width of this power spectral density with that found from Barnes (1980), we find a coherence time of $\tau \sim (\pi \, \Delta f_{\text{fwhm}})^{-1} \sim 4$ sols. While this is not the final quantity that we are seeking, it is an interesting result along the way to deriving the correlation length scale. As an aside, Earth equatorial surface pressure spectra indicate a shorter correlation time, perhaps about 2.5 days (Hamilton and Garcia 1986). The greater correlation timescale for disturbances in the martian atmosphere may make it more predictable than that of the Earth.

We can use the correlation time to estimate the correlation length scale one should find at Mars. Given the phase speeds of the waves on Mars and their correlation times, one can calculate the distances over which the waves would travel while they remain coherent disturbances. This distance is not precisely the same as their instantaneous spatial correlation length, but should be similar to it. By assuming geostrophy between the wind and pressure observations,

Barnes (1980) also computed phase speeds for the waves, with values of about 7 m sec^{-1} in winter and 14 m sec^{-1} in fall and spring at the location of Lander 2. Thus, with correlation times of order 4 sols, correlation length scales of roughly 2300 km (winter) and 4400 km (spring and fall) are expected at this latitude.

Another not entirely unique approach for estimating the correlation length scale can be employed for the second year of Mars Viking Lander data (Barnes 1981). Barnes (1981) again assumed geostrophy between the wind and pressure measurements. From the cross-spectra of the observations, he derived wavenumber frequency spectra for the waves traveling around Mars. He states that the reported variances in the derived zonal and meridional wavenumbers are indicative of the spread of the pressure wavenumber spectrum at a given frequency. Thus, we can use the variances to estimate the width of the wavenumber spectra of these martian disturbances. Then these widths can be used to infer a correlation length, just as the frequency widths are indicative of a correlation time. The values reported by Barnes are a standard deviation in the zonal wavenumber spectra of about 1 wavenumber at 48°N for fall and winter. If that standard deviation is taken to be the half-width at half-maximum of a spectral peak, then a correlation length of about 2000 km is found in the zonal direction at this latitude. Barnes also reports meridional wavenumbers and standard deviations, which we use to infer a meridional correlation length scale. The meridional wavenumber spectra have standard deviations of about 2.5 wavenumbers. This value suggests a correlation length scale of about 1000 km in the meridional direction at this latitude. This result interestingly suggests a possible difference in the length scale depending on the direction in which the correlations are performed. That is, this result suggests that weather is correlated over longer distances in the zonal direction than in the meridional direction at this latitude. Nevertheless, these two values are similar to the values derived using the preceding technique. This is in part a reflection of the fact that both techniques essentially make the same assumptions (geostrophy) in handling the data sets to arrive at the same quantity (the length scale). However, the results are individually interesting as they are from two separate years at Mars. Incidentally, these wavenumber frequency spectra were later compared with GCM simulations by Barnes *et al.* (1993) with good agreement.

We must point out that all of these calculations would also be consistent with a zonally coherent wave propagating past the landers at a varying phase speed. In fact, this may be the preferred explanation, as Murphy *et al.* (1990) looked at the coherence of the signals between the two lander sites and found very high values except during dust storm conditions. Because the landers are separated by nearly 180° of longitude, they interpreted this as indicating that the planetary scale waves seen in the lander data are likely zonally coherent. While there is not enough information in the Viking Lander data sets to completely discriminate between these two scenarios, our analysis of the Viking IRTM data will also address this question.

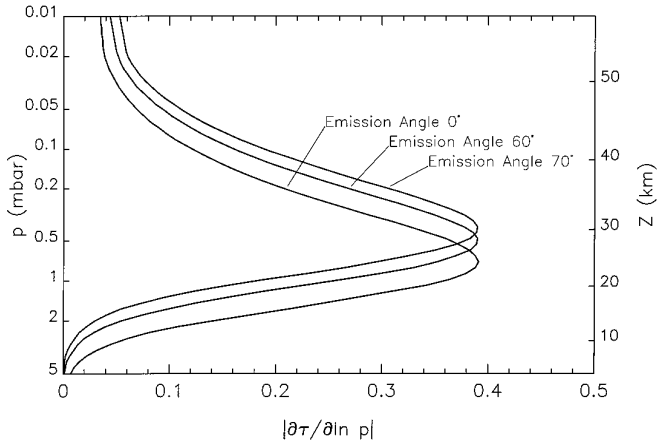

FIG. 1. Weighting functions for the Viking IRTM 15-μm channel measurements. The weighting functions for the emission angles 0°, 60°, and 70° are presented. Note the peak of the 0° emission angle weighting function maximum at around 25 km, and its width of about 2 scale heights. Note also the shift upward in altitude of the weighting function maximum as emission angle increases.

3. VIKING IRTM DATA

The ideal method of determining the weather correlation length scale is to take observations of the whole planet at one time and correlate the weather perturbations with each other. While highly instructive, the Viking Lander data were hardly a *global* data set. The Viking Orbiters had an infrared instrument which was able to sense the atmospheric brightness temperature at a pressure of about 0.6 mbar (about 25-km elevation) in the atmosphere using its 15-μm channel (Martin and Kieffer 1979). In fact, the instrument sensed the thermal radiation emanating from a region of order two scale heights in the vertical, yielding an average brightness temperature for this altitude region (see Fig. 1). The noise level in the data is of order 2 K (Martin and Kieffer 1979). This data set is the focus of this body of work, and we have used it to determine the weather temperature correlation length scale over most of Mars for two seasons. This data set comes closer to the ideal described above, that of a global simultaneous view of the true atmospheric state. While the observations are not both global and simultaneous, there are observations covering nearly half of the globe within an hour. For the weather systems on Mars, observations within an hour of each other should be effectively the same as simultaneous observations. It is, however, also important to note that

the data set from this instrument probes a different region of the atmosphere than that studied by the Viking Landers.

We chose two subsets of the IRTM data to examine in detail, namely 16 weeks centered around $L_S \sim 0°$ (northern spring equinox) and 8 weeks centered about $L_S \sim 180°$ (northern fall equinox). These subsets were chosen because they had the best global coverage of the whole data set and were obtained during times of low dustiness in the atmosphere. Furthermore, seasonal differences between the fall and spring equinoxes might be evident in the analyses. Eventually, data taken during the winter and summer seasons and during dust storms should also be examined in this manner, but was beyond the scope of this work.

3.1. Climatology

The difficulty of using the IRTM data set lies in separating the climatological mean state from the transient weather temperature residuals. In this case, we are using the word climatology to include all of the systematic temperature effects in the atmosphere: seasonal trends, vertical temperature gradients, regional anomalies, and the reproducible daily temperature fluctuations. This climatology will be primarily a function of latitude and time-of-day, reflecting the strong hemispheric and diurnal effects. However, other effects such as emission angle, local topographic elevation, and longitude of the observation can contribute to the systematic variation of the mean brightness temperature observed in the atmosphere. Seasonal effects will present longer-term variations in the climatology, particularly in the latitudinal distribution of mean temperature, and must be considered as well. Thus, our definition of weather is everything left in the data set that is not accounted for with the functionality discussed above. It should include all types of traveling waves, planetary waves, and gravity waves alike. In this section, we will discuss the details of our fit to the climatology of the IRTM data set, with which we have attempted to explain as much systematic variance as possible. It is this climatological mean state that we must remove from the observations to yield the weather temperature effects we are ultimately interested in.

As mentioned above, we expect the atmospheric climatology to be mostly described by functions of latitude and time-of-day. Therefore, the primary component of our least-squares fit to the data will consist of spherical harmonics in latitude and time-of-day. However, we must also consider the emission angle of the observations, as observations taken at higher emission angles actually sample the temperature of the atmosphere at higher altitudes (see Fig. 1). We will model this effect by fitting constant vertical gradients in temperature centered about the mean altitude of the observations. Furthermore, we will allow these vertical gradients to be a function of latitude, but not time-of-day. This assumption is suggested from the work of Santee and Crisp (1992) (and Santee, private communication, 1992) who inverted Mariner 9 infrared spectroscopy (IRIS) spectra to yield temperature profiles of the martian atmosphere. Their results, from one of the same seasons that we examined ($L_S \sim 0°$), suggest that the vertical temperature gradient in the region sampled by the IRTM instrument is essentially constant with altitude and only a function of latitude. We also fit spherical harmonics in latitude and longitude to the data, to allow for topographically fixed waves in the atmosphere. Finally, recognizing the fact that the evolving seasons mean that the climatology is varying with time, we also fit the first time derivative of each of the above terms. It is important to recognize that our spherical harmonics are an orthogonal set of basis functions only for uniformly sampled data. Mathematically, we express our fit as

$$
\begin{aligned}
T_{\text{resid}} &= T_{\text{observ}} - T^{\phi h z \theta}_{\text{mean}} \\
T^{\phi h z \theta}_{\text{mean}} &= \sum_{l=0}^{L_{\max}} \sum_{m=-1}^{l} (T^{\phi h}_{lm} + (t - \bar{t}) \partial T^{\phi h}_{lm}) Y_{lm}(\text{latitude, hour}) \\
&\quad + (z - \bar{z}) \sum_{l=0}^{L_{\max}} (T^{\phi}_{l0} + (t - \bar{t}) \partial T^{\phi}_{l0}) \\
&\quad \times Y_{l0}(\text{latitude}) \\
&\quad + \sum_{l=0}^{L_{\max}} \sum_{\substack{m \neq 0 \\ m=-l}}^{l} (T^{\phi \theta}_{lm} + (t - \bar{t}) \partial T^{\phi \theta}_{lm}) \\
&\quad \times Y_{lm}(\text{latitude, longitude}),
\end{aligned}
\tag{2}
$$

where $z = 0.5 \ln [\sec(\text{emission angle})]$ (Martin and Kieffer 1979) and $\bar{z}$ is the average of that quantity over the period being fit. t is the time that a fit is evaluated at, and $\bar{t}$ is the average time of the data used to produce the fit. The Y_{lm}'s are spherical harmonic functions out to highest order, $L_{\max}$. The $T^{\phi h}_{lm}$ are the fit coefficients of the spherical harmonics in latitude and time-of-day, the T^{ϕ}_{l0} are the fit coefficients in latitude and emission angle, and the $T^{\phi \theta}_{lm}$ are the fit coefficients of the spherical harmonics in latitude and longitude. The ∂T terms are the corresponding time derivatives of the preceding spherical harmonic coefficients referenced to $\bar{t}$. The spherical harmonics expressing the fit in terms of latitude and longitude do not include the $m = 0$ terms as those are redundant with the $m = 0$ terms of the latitude and time-of-day spherical harmonics.

To maintain quality in the data and the fits, filtering was done on IRTM's quality flag, emission angle, and local topography of the observations. Only observations tagged with an IRTM quality flag less than 4096 were considered. This represents data with the only potential flaw being unremoved spikes (see Kieffer 1989, PDS Viking IRTM CD-ROM, IRTM.TXT). The emission angle was limited

to below 65°, effectively limiting the vertical extent sampled by the observations. Above this, the constancy of the vertical derivative became suspect. Martian atmospheric optical depth in the 15-μm band is about 1 at 25 km, yet topographically high regions of Mars reach this elevation. The possibility arises of observations contaminated by surface radiance. The surface contribution to the measured radiance in the 15-μm band from regions of elevation below 12 km should be less than 8% of the total radiance (Mike Smith, personal communication, 1995). Observations taken over locations topographically higher than this will likely be significantly contaminated by surface temperatures, and thus need to be discarded. We chose 12 km as the cutoff, because only a very small portion of the planet is then excluded (Tharsis volcanos and Olympus Mons) and the surface contribution drops off very quickly below that altitude.

Because we also fit for the time derivatives of the climatology, we were able to use data over longer periods to specify the fit. In particular, we were able to compute a single fit for all of the data in the longer (16-week) subset about $L_S \sim 0°$ that we analyzed. Using this full time to compute the fits allowed the coverage to be better than that which would have been achievable with a shorter time fit that did not account for time derivatives. In fact, however, we broke the 16-week segment up into two 8-week interleaved data sets to have two related yet independent data sets to compare. We combined weeks 1–2, 5–6, 9–10, and 13–14 into one data set and then weeks 3–4, 7–8, 11–12, and 15–16 into another data set, and then analyzed them separately to compare the consistency between the results. This still allowed for good coverage, yet a clear indication of the repeatability of the results. We did not break up the 8-week segment of data around $L_S \sim 180°$, but rather analyzed it as a whole. Estimates of errors in the analysis of that portion were inferred from the results at $L_S \sim 0°$. We estimate a value of about 1 K accuracy in our fits by comparing two similarly good fits, e.g., an $L_{max} = 7$ fit and an $L_{max} = 6$ fit. Their differences in the regions in which there are data are less than about 1 K. Figure 2 shows the coverage allowed in an 8-week period of the IRTM data at $L_S \sim 0°$ that we have analyzed.

Figure 3 shows the climatological mean state at one time for a few particular latitudes. The figure also shows some of the raw data from which the climatology was derived. Keep in mind that the weather temperature fluctuations are present in the data, but not in the climatology fits. We will show later how the weather temperature fluctuations are of order 6 K^2, while the sum of the errors in the climatology fits and the observational errors are of order 4 K^2. Thus, this does in fact show good agreement between the data and the climatology in the regions in which there are data.

We computed fits out to $L_{max} = 15$, yet found that $L_{max} = 5$ was always sufficient. That is, the terms which most decreased the χ^2 of the fit were all $L_{max} = 5$. Figure 4a shows an $L_{max} = 5$ fit in latitude and time-of-day to the 16-week period of the data around $L_S \sim 0°$. Most noticeable in this fit is the diurnal component of the daily temperature oscillation. It reaches a peak at about 13 H (1 H is defined as 1/24th of a sol), or just after local noon. The amplitude of this diurnal tide is roughly 12 K at the equator, although it is difficult to separate the diurnal tide from the semidiurnal tide in this representation. The semi-diurnal component is also noticeable, although the large cold area in the atmosphere at 22 H around the equator is mainly due to a hole in the coverage of the data (see Fig. 2a). The atmospheric cooling toward the poles is also prominent in this plot, with a difference of 45 K between the highest equatorial temperature and the coldest polar temperature. Again, this fit (and thus, the tidal amplitudes) is roughly within 1 K of the actual climatology of Mars' atmosphere at this altitude and season in regions which were well sampled by the IRTM instrument. Clearly there is much information in these fits about the structure, amplitude, and phase of the thermal tides in the martian atmosphere at this altitude. However, a detailed analysis is beyond the scope of this paper, but will be explored in later work.

We also fit terms in latitude and longitude to the data, to represent phenomena like stationary waves in the atmosphere. The same fit that was shown above as a function of latitude and time-of-day can be also portrayed as a function of latitude and longitude. This is shown in Fig. 4b. Remember that the $m = 0$ terms are redundant with those in the spherical harmonics for latitude and time-of-day, and thus are not included in the latitude and longitude representation of the fit. That is why the azimuthally averaged latitudinal temperature gradients do not show in this plot. Of note in this figure is the predominant $m = 1$ mode in the southern mid-latitudes, and the $m = 2$ mode in the northern mid-latitudes. This is strikingly similar to the results found by Hollingsworth and Barnes (1995) and by Nayvelt (private communication, 1995) for $L_S \sim 270°$. They both have models which predict such a hemispheric distribution of zonal modes, although the absolute phases differ among their works and ours. While it is of question whether comparing our results with model results from different seasons is valid, the similarities are encouraging. We will present further analysis of these and additional observations of stationary waves in a later work.

After subtracting the climatological fits from the data, scatter plots of the residuals were used to check for any systematic variation left as a function of any of the independent variables, i.e., emission angle, latitude, longitude, local topography. No apparent correlations were found in any of the independent variables. Thus, the combination of the

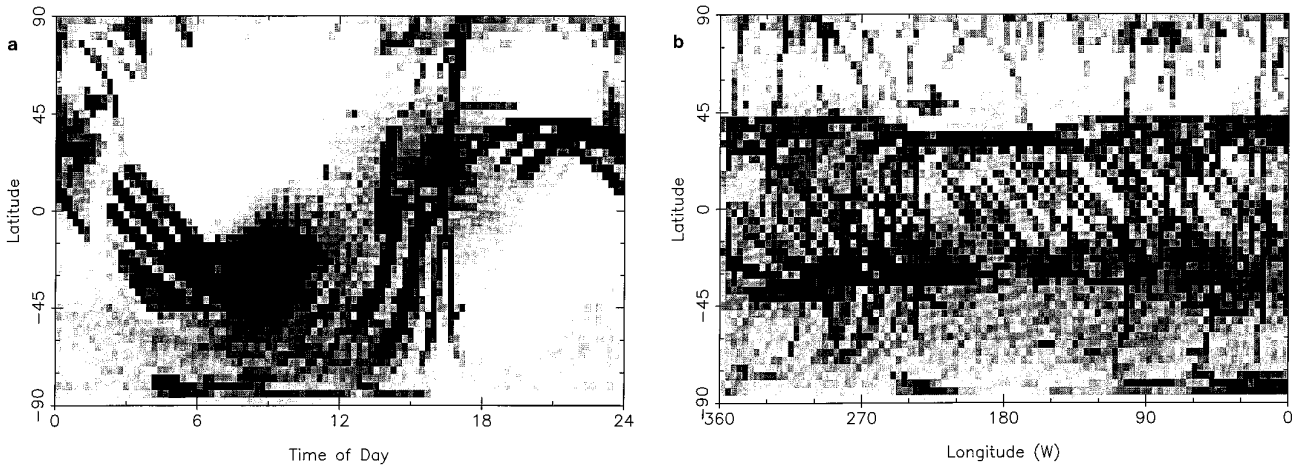

FIG. 2. The coverage afforded by Viking IRTM observations from JD 3400-3512 (Northern spring equinox, $L_S \sim 0°$) in (a) latitude and time-of-day and (b) latitude and longitude. In (a), the number of observations in this period is binned by 3.6° latitude and 0.24 H, with values ranging from 0 to 963 per bin. The gray scale is adjusted so that white represents a data gap (no observations) and it saturates to black at 100 observations per bin. Note the poor coverage in the North, and at certain times-of-day farther South. In (b), the number of observations is binned by 3.6° in both latitude and longitude, with values ranging from 0 to 799 per bin. The gray scale is adjusted so that white represents a data gap and it saturates to black at 100 observations per bin again.

data filtering and the functionality of our fits adequately describes the systematic variation in the data set.

3.2. *Weather Correlations*

For each datum, its departure from local climatology is now the part of the data set we are interested in. Having derived the climatological mean state, we then subtract it from the raw data to leave the observational residuals, T_{resid}. In this section, we will discuss how we compute the weather temperature correlations and their variances from these residuals, as well as present the results of these calculations.

We had to choose a time window in which we could consider observations to be simultaneous, at least from the perspective of trying to correlate moving weather systems. As mentioned previously, we can expect a phase speed of these systems of roughly 20 m sec^{-1} (at least in the mid-latitudes) (Barnes 1981). Our previous simple estimates of the weather correlation length scale suggest a length scale

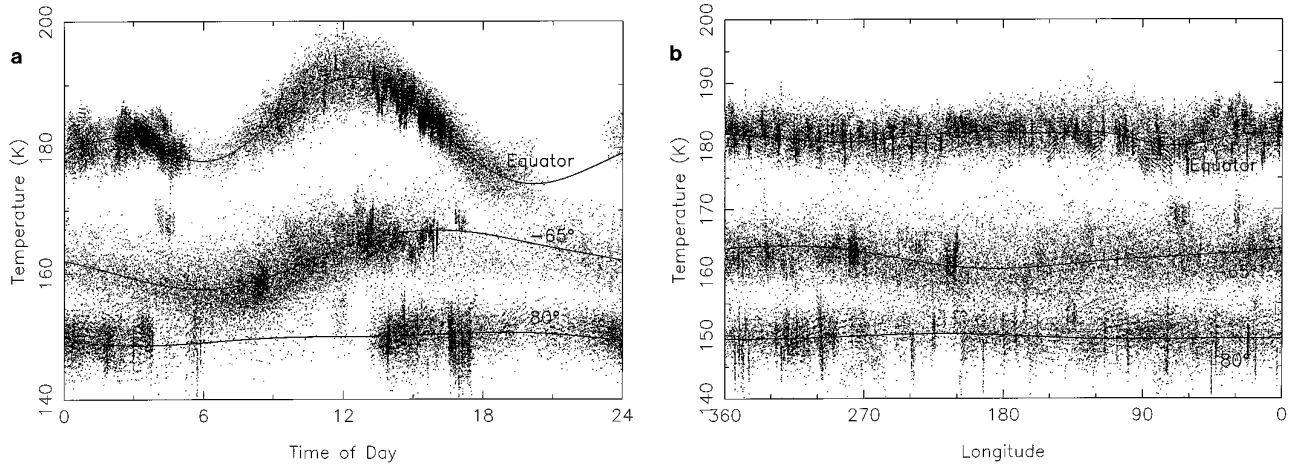

FIG. 3. A comparison of the climatology fit and the data used to derive it for JD 3400-3512 of the Viking IRTM T15 data. Shown on this plot are cross sections of the global fit at three latitudes: the equator, 65°S, and 80°N. Note the good accord between the data and the fits in regions in which there are data. The discrepancies between the fit and the data mainly represent the weather temperature variations we are primarily interested in. In (a) the abscissa is time of day, while in (b), it is longitude.

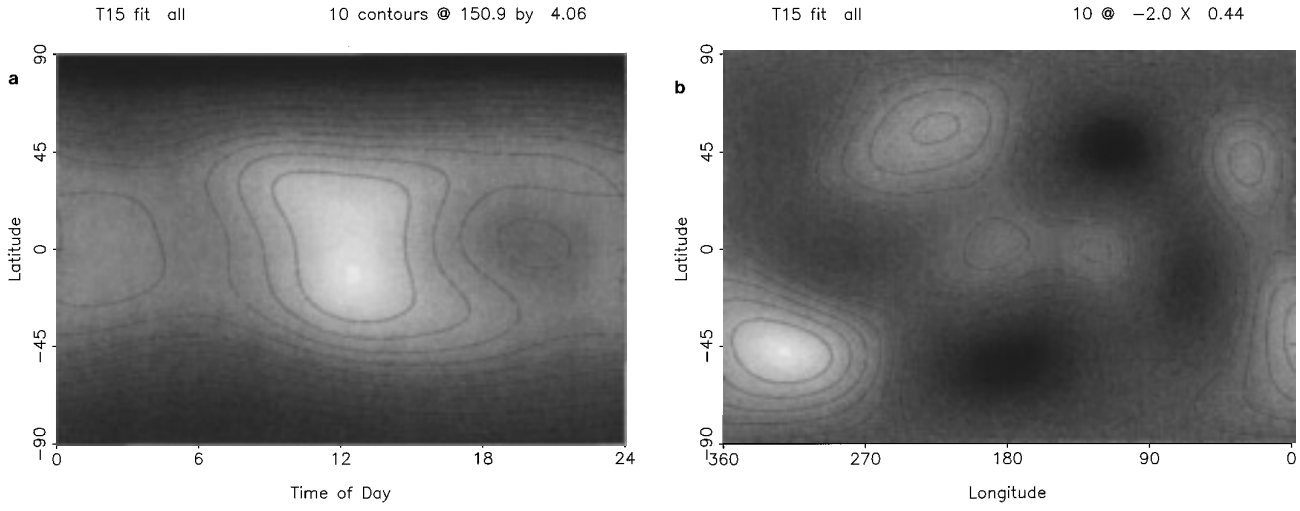

FIG. 4. A fit to the 16 weeks of data from JD 3400-3512 as a function of (a) latitude and time-of-day and (b) latitude and longitude. Dark represents hot, and the contours in (a) are between 147 and 191 K, spaced by about 4.0 K. This fit is in spherical harmonics out to $L_{max} = 5$. The diurnal variation has an obvious peak near the equator at a time-of-day just slightly after local noon. The rough latitudinal symmetry is indicative of this period being near equinox ($L_S \sim 0°$).

at least of order 2000 km. We can consider two observations of a weather system simultaneous if it has moved only a small fraction of its own size in the time between the observations. So as not to automatically select out the same length scale as previously estimated we will use conservative estimates to determine an acceptable time window. If we require a 500-km disturbance to move less than one-fifth of its size, it could only move 100 km. If it is traveling at 30 m sec^{-1}, this means it could go for about 1 hr before it propagated 100 km. Thus, we use a window of 1 hr during which we consider observations to be simultaneous. We also tried performing all the calculations with a time window of 3 hr, which negligibly changed the results.

We separated the data into nine bins organized every 20° of latitude, and then separately analyzed the data in each bin. We computed the variances of the observational residuals, T_{resid}, in each of the bins

$$\sigma^2(\phi) = \langle T_{resid}(\phi)^2 \rangle - \langle T_{resid}(\phi) \rangle^2. \quad (3)$$

In this notation, ϕ represents the latitude bin of interest, $T_{resid}(\phi)$ represents all the observational residuals in that bin, and the angled brackets $\langle\ \rangle$ represent taking the mean over the ensemble of data. We also computed the covariances of the observational residuals with all others in that bin which were taken within 1 hr of the first. We computed these covariances in 50-km bins determined by the great circle separation distance between the two observations

$$\mathrm{cov}(\phi, d) = \langle T_{resid}(\phi)_i T_{resid}(\phi)_j \rangle - \langle T_{resid}(\phi)_i \rangle \langle T_{resid}(\phi)_j \rangle, \quad (4)$$

where d is the separation distance between the two observational residuals, $T_{resid}(\phi)_i$ and $T_{resid}(\phi)_j$. Attempts were made to also compute the covariances as a function of the azimuth angle from north between two observations, but poor results were found and will not be reported here. Furthermore, covariances were computed using the separation in the zonal direction only (measured from the center latitude of the bin) as the separation distance, under the expectation that weather might display greatly different correlation length scales in the zonal versus meridional directions. The results of this differed very little from covariances computed using the great circle distance as the separation and will not be presented separately. Remember that we computed covariances only within 20° latitude bins (i.e., ~1000 km latitudinally), so our separation distances are predominately in the zonal direction anyway due to the shape of the bins.

The above equations define how we calculated the observational residual variances and covariances. However, the weather temperature covariances (and variances) that we are interested in for correlations are not simply the products of the observational residuals with each other. In fact, the observational residuals have another component in addition to the weather temperature residuals: the observational errors,

$$T_{resid} = T_{wx} + \sigma_{obs}. \quad (5)$$

The observational errors are not small ($\sigma^2_{obs} \sim 3\ K^2$) and must be considered. They are a function of the temperature of the observation as the detector sensitivity changes with

observed temperature. They can be assumed to be uncorrelated from one observation to the next, as they are primarily due to detector noise (Chase *et al.* 1978), but they will certainly correlate with themselves. Thus, the product of an observational residual with itself, i.e., an observational residual variance, will have a term from the observational error variance, while the covariances in general will not.

Mathematically, we can express the above by:

$$\sigma^2(\phi) = \sigma^2_{\text{wx}}(\phi) + \sigma^2_{\text{obs}}(\phi), \tag{6}$$

where the subscript "wx" represents the true weather temperature residuals, and "obs" represents the observational error. Thus the observational residual variance contains not only the weather temperature residual variance, but also the observational error variance:

$$\text{cov}(\phi, d) = \text{cov}_{\text{wx}}(\phi, d) + \sigma^2_{\text{obs}}\delta(d). \tag{7}$$

The covariance of the observational residuals with one another is composed of a part due to the covariance of the weather residuals and a part due to the observational error variance at zero separation.

The correlations that we are ultimately after are composed only of the covariances and variances of the weather residuals:

$$\rho(\phi, d) = \frac{\text{cov}_{\text{wx}}(\phi, d)}{\sigma^2_{\text{wx}}(\phi)}. \tag{8}$$

We could model the error terms in order to remove them from the covariances (and variances). However, we chose not to do this, as our ability to model these terms is poor and would likely introduce significant errors into our weather temperature variance and correlation estimates. Instead, we remove the observational error variances from the total variances using the idea that the weather correlations should approach 1.0 at zero separation. Unless there are significant very small scale structures in the weather, the weather correlations should smoothly rise to unity at the origin. Thus, by requiring this of the correlations, we can implicitly remove the observational error variances without modeling them. We have performed this by extrapolating the original correlations at 25 and 75 km separation to zero separation. Then the weather temperature variances were adjusted so that this correlation at zero separation was 1.0. We did attempt to separately estimate and remove the observational error variances from the observational residuals and found results quite similar to those found by extrapolating the correlations to zero separation. We believe that the extrapolation technique corrected the results most accurately.

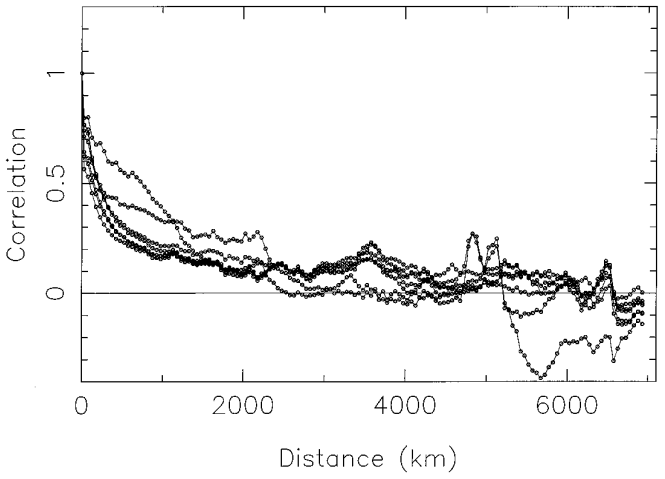

FIG. 5. Correlations as a function of distance for a particular latitude band and 14-sol period of the Viking IRTM T15 data. The seven curves on the plot represent different spherical harmonic truncations in the model of the climatology. The four curves which are nearly superimposed on one another are for $L_{\text{max}} = 10$, $L_{\text{max}} = 7$, $L_{\text{max}} = 6$, and $L_{\text{max}} = 5$, suggesting that these climatology fits all adequately describe the climatological variations. The other three curves which all differ are for $L_{\text{max}} = 4$, $L_{\text{max}} = 3$, and $L_{\text{max}} = 2$, suggesting that these climatology fits have insufficient resolution to adequately describe the climatological variations.

We ignored the climatological fit errors in our calculations. Although the errors in the climatology fit are small compared to the variance of the weather temperature residuals, there was concern that our correlation length scales might simply represent the smallest length scales in the fits. Here we show that the climatological fit error covariances are insignificant in terms of the correlations. We did this by computing the correlations using climatology fits of differing length scales, namely $L_{\text{max}} = 2$, $L_{\text{max}} = 3$, $L_{\text{max}} = 4$, $L_{\text{max}} = 5$, $L_{\text{max}} = 6$, $L_{\text{max}} = 7$, and $L_{\text{max}} = 10$. The results were that the correlations of the $L_{\text{max}} = 5$, $L_{\text{max}} = 6$, $L_{\text{max}} = 7$, and $L_{\text{max}} = 10$ fits were nearly identical (as were the largest terms in the fits), but the $L_{\text{max}} = 2$, $L_{\text{max}} = 3$, and $L_{\text{max}} = 4$ fits differed significantly from the others. A sample of these correlations are shown for a particular latitude band and 8-week subset of the data in Fig. 5. Thus, we conclude that our correlations are measuring the weather temperature correlation length scale, not the climatological fit error covariances. This also indicates again that the climatology fits can be adequately described by a fit with $L_{\text{max}} = 5$. Ignoring the climatological fit errors has likely caused us to overestimate the weather temperature variances by roughly 1 K^2, a marginally significant amount.

As an example of the correlations computed, in Fig. 6 we present the results for the latitude band centered at 20°N at $L_S \sim 0°$. This latitude band encompasses the Viking Lander 1 site, and thus is instructive for comparisons with

the Lander results. The heavy lines on the figure show the correlations from both the first and second group of observations analyzed at this season. The differences between these curves are indicative of the reproducibility of the results, and thus the errors in the correlation curves. While the curves are not identical, they do follow a similar trend out to about 2000 km. Beyond there, the curves are less similar, primarily due to the fact that fewer covariance pairs were calculated at the longer separation distances, increasing the noise in the calculation. The number of covariance pairs is also plotted on this figure, as the light dotted lines near the top of the plot. They are plotted logarithmically, with a scale on the right-hand side of the plot. The correlation curves show an exponentially decreasing correlation, with a characteristic length scale of about 600 km, similar to the simple estimates presented above. Also shown on the plot, as a dashed line, is an exponential fit to the curves which will be discussed later.

Figure 7 shows these same correlation curves for all of the latitude bins for the first and second groups of correlations around $L_S \sim 0°$. Again, the two solid lines are not identical but follow the same trends. In general the correlations are all falling off roughly exponentially with a characteristic length scale of order 1000 km. However, there do appear to be significant differences in the curves between different latitudes. These differences are in the shape of the correlation and also in its overall length scale. We do not attempt to quantify or explain the shape differences here, as those are at least in part due to noise in the correlation calculations. However, we do examine the overall length scale variations.

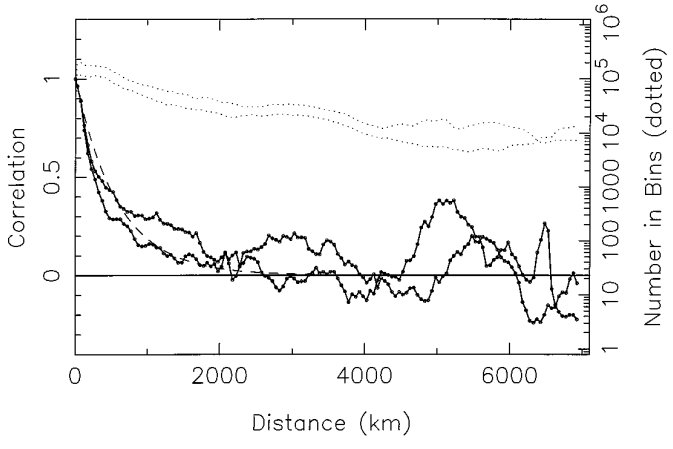

FIG. 6. Correlation as a function of separation distance for the latitude bin centered on 20°N. The solid lines are the correlations computed for the two groups of data around $L_S \sim 0°$. The dotted lines represent the log of the number of individual covariances averaged in each 50-km bin for the two groups. There are roughly 10^5 individual covariances in each bin, reducing the noise on each correlation curve. The correlation drops like an exponential with a characteristic length of order 1000 km. A fit to this exponential dropoff is represented by the dashed line.

We fit exponentials of the form $\rho = e^{-kd}$ to the correlation curves, where k is a fit parameter and d is again the separation distance. We weighted the fits by the number of covariance pairs in each bin to produce a weighted least-squares fit to each of the curves. For the $L_S \sim 0°$ subset, this yielded values for each 20° latitude bin from north to south of 240, 670, 660, 600, 1200, 640, 900, 2500, and 1800 km, respectively. The numbers listed here are an average of the two results from the first and second groups analyzed at $L_S \sim 0°$. The results suggest that there is perhaps a shorter length scale in the north than in the south.

Figure 8 shows the correlation curves for the northern fall equinox season ($L_S \sim 180°$). In this case, we only computed one group of correlations for this season, so the errors in these correlations can only be estimated from those found in the opposite season. As the coverage was somewhat worse during the northern fall equinox, the errors are probably slightly larger for this subset. Nevertheless, one again sees similar general behavior in these plots, namely, a dropoff of order 1000 km, perhaps being shorter in the north.

In fitting exponentials as above to these correlations, we found characteristic length scales of 400, 380, 460, 880, 730, 990, 1000, 940, and 790 km for each 20° latitude bin going from north to south. These estimates again support a shortening of the length scale towards the north as was seen during the $L_S \sim 0°$ season.

We have compiled these weather correlation length scale determinations in Fig. 9. For the $L_S \sim 0°$ results (solid lines), which show a significant range of values for each latitude bin, we have indicated the values found in each of the two subsets of data analyzed. For the $L_S \sim 180°$ results (dotted line) we only show a single point for each latitude bin. In this plot, it is clear that the northern latitudes consistently show smaller weather correlation length scales, while the south exhibits generally larger length scales for both seasons analyzed.

We also examined the magnitude of the weather temperature variance. Figure 10 depicts the weather temperature variance as a function of latitude for the two groups analyzed around $L_S \sim 0°$ (solid line) and the one group centered on $L_S \sim 180°$ (dotted line). The differences between the solid curves are indicative of the errors present in this calculation, which are significant particularly near the equator. These results suggest that in both seasons, there are large weather temperature variances near the south pole, and also near 60°N; each with variances of order 5–10 K^2. The inconsistency of the two solid curves near the equator makes it difficult to conclude anything about the weather temperature variance there aside from a rough magnitude of perhaps 4 K^2. Again, recognize that by ignoring the climatological fit error variances, we are likely overestimating these weather temperature variances by about 1 K^2.

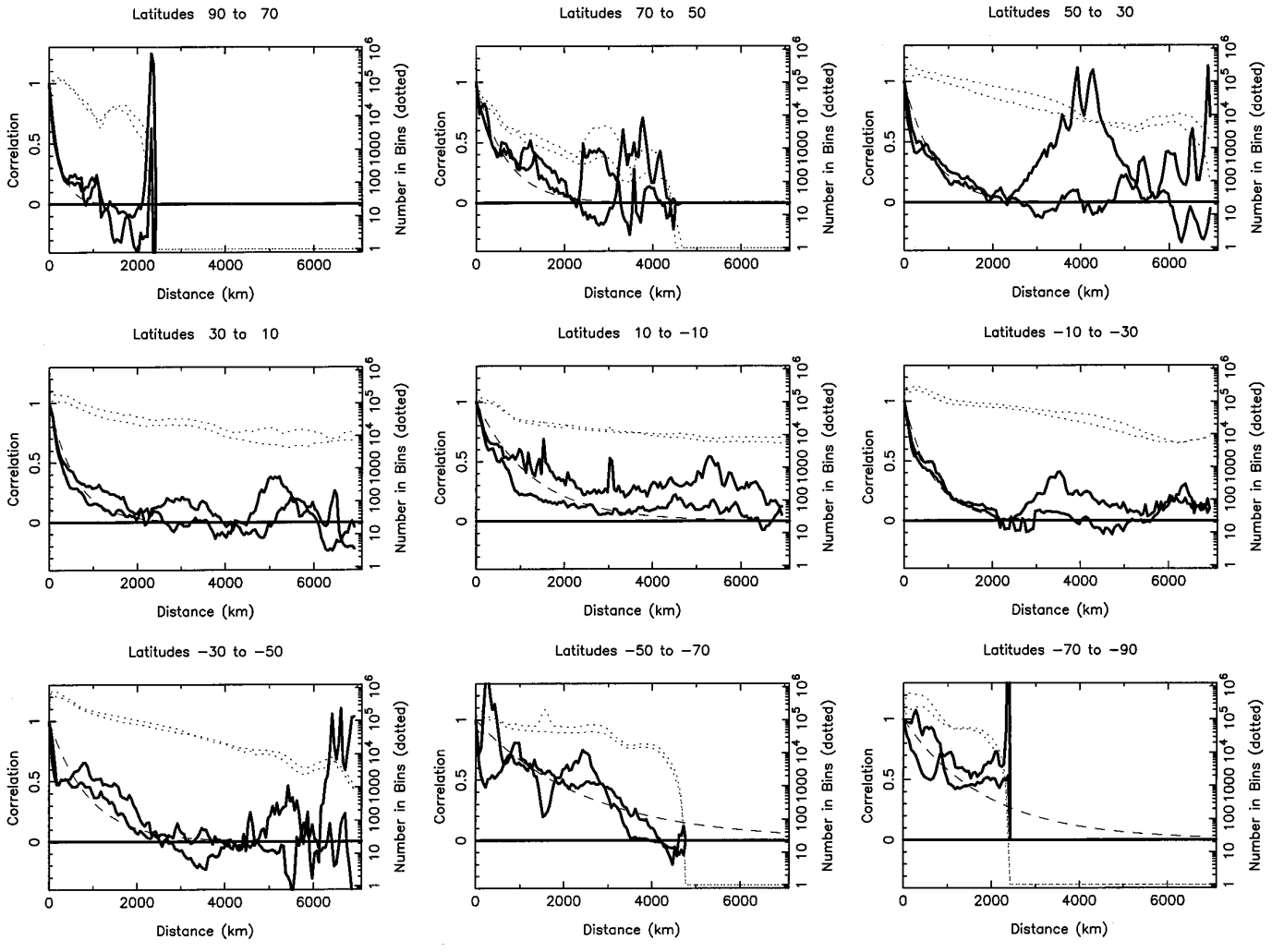

FIG. 7. Correlation as a function of separation for all of the latitude bins for the two groups of data analyzed around $L_S \sim 0°$. The structure of each plot is the same as that of Fig. 6. Note the similarities between the two solid lines in each plot, and the differences in overall length scale and shape of the correlation curves among the different plots. The differences between the two solid lines on each plot are indicative of the errors present in these calculations.

4. DISCUSSION

In this section, we summarize our determination of the weather correlation length scale. We also suggest some explanations for details observed in the correlation curves, and what that might suggest about the weather of Mars. Furthermore, we compare our determinations of the weather temperature variances with published results from GCM simulations and other data sets. Finally, we use our length scale estimates to suggest the number of landers necessary to observe well the global atmospheric state of Mars.

We have summarized our weather correlation length scale determination from IRTM data and estimates from other techniques in Table I. The results seem to show a large variety of length scales. That is, the Viking Lander results suggest length scales ranging from as low as about 1000 km to as high as the full circumference of the planet. The IRTM results of this work suggest lengths of between 250 and 2700 km, partially overlapping the Lander results, but significantly shorter in general. Theory suggests a number of order 1000 km, barely overlapping both the Lander and IRTM results.

We could explain the differences in these varied results as due to the large uncertainties present in all of the calculations. Factors of at least two appear to be present as uncertainties in all of the data analysis results. However, it is also possible that the differences are real and due to some intrinsic difference between the data sets. This is perhaps due to one or more of several reasons, the most obvious of which is the fact that the data sets were obtained from different altitudes in the atmosphere. The Viking Landers

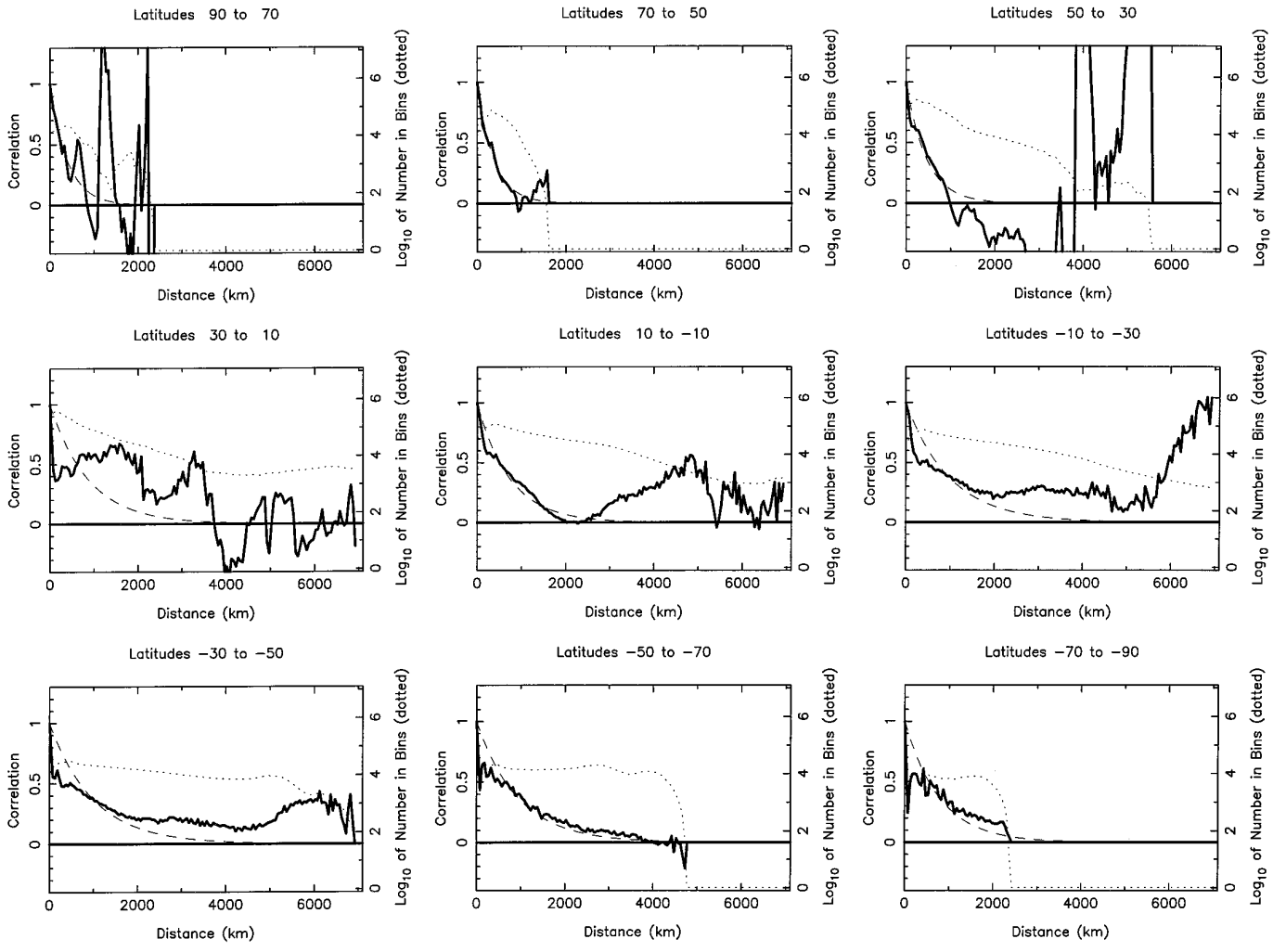

FIG. 8. Correlation as a function of separation for all of the latitude bins for the data analyzed around $L_S \sim 180°$. The structure of each plot is the same as that of Fig. 6. Note the general falloff in about 1000 km, and the latitudinal differences. Compare this figure with Fig. 7.

were in the planetary boundary layer, while the IRTM observations correspond to an altitude of about 25 km. It is possible that both data sets were seeing planetary scale waves, but that these waves' coherence lengths varied with altitude. It is also possible that while the Viking Lander data analysis was seeing planetary scale waves, the IRTM observations may have been dominated by smaller scale waves, such as gravity waves.

Should the 25-km altitude brightness temperature observations of IRTM T15 yield similar weather correlation length scales as the surface pressure observations of the Landers? If one accepts that our IRTM results are showing the same relatively incoherent planetary scale waves as the Lander results, then this agreement can in itself tell us something of the nature and vertical extent of Mars' weather. That the two different meteorological quantities (pressure and temperature) yield similar results indicates that the weather phenomena are similarly manifested in both pressure and temperature variations for Mars. It also implies that the weather phenomena investigated have large vertical extents, i.e., extending over at least two scale heights. This hypothesis is generally supported by GCM calculations reported in Barnes *et al.* (1993). In that work, they also discuss the vertical structure of the eddies observed in their model runs. They most often (but not always) find eddies which are vertically coherent over the full domain of the model, namely about 4 scale heights. This behavior was also previously observed in the martian atmosphere by Conrath (1981) who analyzed Mariner 9 IRIS spectra. He observed an atmospheric disturbance which had both a consistent frequency spectra and phase structure with height up to about 4 scale heights as well. Therefore, we do not find it surprising that the length scales we derive from these different data sets (and regions of

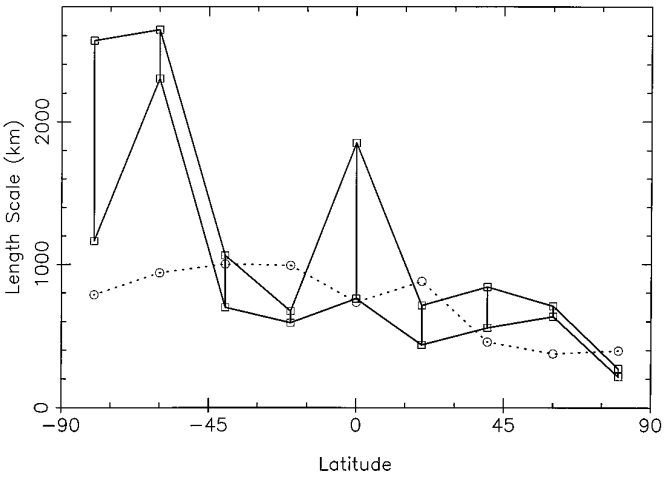

FIG. 9. Weather temperature correlation length scales as a function of latitude for $L_S \sim 0°$ (solid lines) and $L_S \sim 180°$ (dotted line). The vertical solid lines connect the extrema of the length scales found for each latitude bin for the $L_S \sim 0°$ subsets, showing roughly the reliability of these values. Only one subset of $L_S \sim 180°$ was analyzed so no ranges are shown for those values. All these values were determined by fitting exponentials to the correlation curves in Figs. 7 and 8. Note the smaller length scales in the north.

the atmosphere) are roughly similar. It is still possible that the spatial coherence of these waves changes with altitude, and it is likely that the same waves are being observed at the surface and at altitude. The differences in the length scales as seen by the Landers and our IRTM analysis are

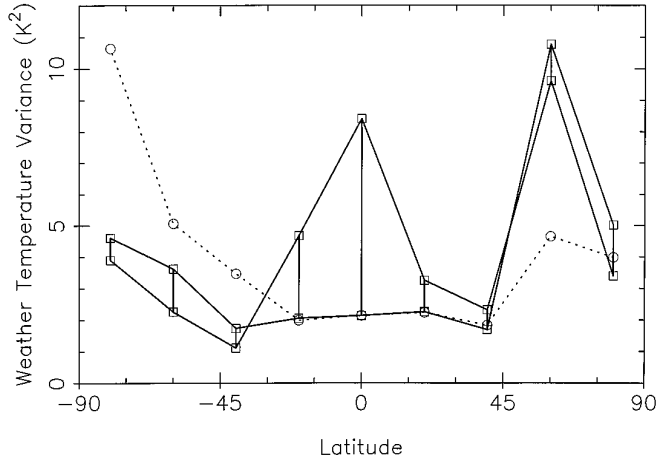

FIG. 10. Weather temperature variance as a function of latitude for the two groups around $L_S \sim 0°$ (solid lines) and the group around $L_S \sim 180°$ (dotted line). These curves represent the variance in the temperature at the 0.6 mbar level caused by weather phenomena on Mars. The differences between the two solid curves are indicative of the errors in these results, which are significant. For the two groups at $L_S \sim 0°$, global average values of ~4 K^2 are found, while for $L_S \sim 180°$, a value of about 3 K^2 is found.

TABLE I
Martian Weather Correlation Length Scale Estimates

Technique	Length (km)
Theory	$L_D(45°) \sim 1000$
Lander $V \cdot \Delta t$	2300–4400
Lander Δk	1000–2000
Landers coherence	Global?
This work	250–2700

then probably either due to such a change in spatial coherence with altitude or simply the uncertainties in the analyses.

We noted an apparent latitudinal dependence in our estimates of the weather temperature correlation length scales (see Fig. 9). This was manifested as a decreasing length scale toward the north pole. Such a phenomenon was noted in the Earth's atmosphere by Ghil *et al.* (1979), who examined prediction error correlations for use in data assimilation. They explained it in terms of the variation of the Rossby radius with latitude. Recall that the Rossby radius can be expressed by $L_D = NH/2\Omega \sin \phi$, and so decreases with increasing latitude (ϕ). This phenomenon has also been observed in eddies in the Earth's oceans as reported in Krauss *et al.* (1990). This explanation is appropriate to Mars if the short correlation length scale weather variations are due to non-planetary scale waves which are generated at the latitudes where they are observed. Mars, however, also has planetary scale waves with meridional extents on the order of the radius of the planet, and thus these waves are not discrete eddies separated in latitude as in the Earth's ocean. Therefore, an explanation which is perhaps more valid for this type of wave on Mars involves simply the shortening of zonal scales with increasing latitude. The length scales measured from a meridionally large system will decrease with latitude simply due to the shortening of latitude circles, scaling like $\cos \phi$. Thus, because these two equally valid explanations exist, the variation of the weather correlation length scales with latitude is not particularly diagnostic. That is, we cannot discriminate between relatively incoherent planetary scale waves or non-planetary scale waves generating short correlation length scales.

It is interesting that we do not see a symmetric distribution of length scales about the equator in these equinoctial observations. Although the southernmost latitude bin also showed slightly shortened length scales, the decrease was much less dramatic than in the north. This trend was the same for both $L_S \sim 0°$ and $L_S \sim 180°$, not reversing between fall and spring as might be expected. Thus, the hemispheric asymmetry of the weather correlation length scales is not

just a seasonally controlled phenomena and is probably due to persistent hemispheric differences in the weather.

The weather temperature variances computed in our IRTM analysis also can be compared with other published work. Barnes *et al.* (1993) report the GCMs transient eddy temperature variance as a function of latitude and altitude. At $L_S \sim 0°$ (their Fig. 18), near 25-km altitude, they report variances of between 0.5 K^2 and 3 K^2, with a globally averaged value of about 1 K^2. Our results were consistently higher than this, with a globally averaged value of about 4 K^2 for the season, and peaks up to about 10 K^2. The match is good only to an order of magnitude level. At $L_S \sim 180°$ (their Fig. 16), near 25-km altitude, they report variances of between 0.5 K^2 and 11 K^2, although values above 4 K^2 are found only between 40°N and 65°N. A globally averaged value of their findings is roughly 2.5 K^2. For this season, we again found values slightly higher than this, with a globally averaged value of about 3 K^2. While we caution against over-interpreting the latitudinal structure in our weather temperature variance results; for $L_S \sim 180°$, we do see greater values north of 40°N. This hints at an agreement with the GCM results, in spite of the magnitude differences and the fact that we also see strongly elevated weather temperature variances near the south pole. The magnitude differences can only be partially explained by the probable 1 K^2 overestimate caused by ignoring the climatological fit error variances in the calculations.

As another comparison for our variance calculations, Conrath (1981) also computed a temperature amplitude from a wave he observed in Mariner 9 IRIS data. While his data set is from a time slightly earlier ($L_S \sim 340°$) than our northern spring equinox subset ($L_S \sim 0°$), it is still useful to compare against. He found wave amplitudes of up to 4 K at the 25-km altitude, in a latitudinally confined region between about 50°N and 70°N. This observation is quite consistent with our findings for this season. We see an elevated band of weather temperature variance centered on 60°N with a magnitude of about 10 K^2.

The remaining magnitude differences between our results and those of the GCM may be due to the fact that the GCM results represent only the transient eddy temperature variance, as other variations were filtered out before the analysis. Our results include this contribution, as well as gravity waves and perhaps unremoved noise sources such as intermittent stationary waves or deficiencies in our fit to the thermal tides. Thus, it is not surprising that in general our weather temperature variances are greater than those seen in the GCM simulations. The magnitude differences imply that these other phenomena are likely a substantial component of the IRTM T15 measured transient temperature variations. However, they are not likely to be the dominant signal. Perhaps also, the variance magnitude differences are in part due to shortcomings of the current GCMs.

Seaman (1977) showed that the accuracy in estimating the atmospheric state from a network of landers is directly related to the spacing of landers divided by the weather correlation length scale. Thus, one can estimate the optimal number of landers on Mars to observe the global surface pressure without missing any significant features in the weather signal. If one accepts that our correlation length scales represent the length scales one would measure at the surface then we can use the length scales to help plan a global network of landers. If one takes the smallest length scales in each latitude bin for either season investigated and sets the separation of landers to that, one finds a total number of order 100 landers is optimal. It is the small length scales found in this analysis that suggest such a large number of stations to completely observe Mars' transient phenomena. However, if the shorter correlation lengths we have found are not representative of what would be found at the surface, then this is not a good technique to use to plan a network of landers. If the planetary scale waves observable at the surface are truly zonally coherent as suggested by Murphy *et al.* (1990), then a relatively small number (of order 10) could well observe these waves in the bottom of the atmosphere for the whole planet.

5. SUMMARY

In analyzing the Viking IRTM T15 data sets to derive the weather temperature correlation length scales, we have established another benchmark with which to compare the current crop of martian GCMs to the realities of the martian atmosphere. We found length scales for the correlation of order 100 km, and indications that it has an interesting latitudinal structure (smaller in the north). We found weather temperature variances at 25 km altitude of about 4 K^2 ($L_S \sim 0°$) and 3 K^2 ($L_S \sim 180°$), somewhat higher than that found in model calculations (e.g., Barnes *et al.* 1993) but similar to that found in another data set (e.g., Conrath 1981). This is perhaps due to the fact that our analysis was sensitive to all sorts of traveling waves, while the model analyses were only sensitive to planetary scale waves. The weather correlation length scales derived here should be useful in developing the first operational atmospheric data assimilation systems for Mars, when global data become available. These length scales may be used as a guide in determining the density of landers to comprise an optimal meteorological network for Mars. The in-depth analysis on the IRTM data was only performed during the non-dusty times around spring and fall equinox. However, both Lander observations and GCM calculations suggest that perhaps the most interesting time to study weather phenomena is during the winter season, when the temperature variances increase by perhaps a factor of two. There-

fore, to add to this work, to better constrain the optimal number of meteorological landers for Mars and to further understand the nature of weather on Mars, we plan to eventually perform this type of study throughout the whole of the IRTM data set.

ACKNOWLEDGMENTS

The authors acknowledge the helpful input of two anonymous reviewers, both of whom suggested significant improvements to the analysis technique presented in this paper. This work was funded by the Mars Observer Project and the NASA Planetary Atmospheres Program.

REFERENCES

Banfield, D., A. P. Ingersoll, and C. L. Keppenne 1995. A steady-state Kalman filter for assimilating data from a single polar-orbiting satellite. *J. Atmos. Sci.* **52,** 737–753.

Barnes, J. R. 1980. Time spectral analysis of midlatitude disturbances in the marian atmosphere. *J. Atmos. Sci.* **37,** 2002–2015.

Barnes, J. R. 1981. Midlatitude disturbances in the martian atmosphere: A second Mars year. *J. Atmos. Sci.* **38,** 225–234.

Barnes, J. R. 1984. Linear baroclinic instability in the martian atmosphere. *J. Atmos. Sci.* **41,** 1536–1550.

Barnes, J. R., J. B. Pollack, R. M. Haberle, C. B. Leovy, R. W. Zurek, H. Lee, and J. Schaeffer 1993. Mars atmospheric dynamics as simulated by the NASA Ames general circulation model. 2. Transient baroclinic eddies. *J. Geophys. Res.* **98,** 3125–3148.

Chase, S. C., Jr., J. L. Engel, H. W. Eyerly, H. H. Kieffer, F. D. Palluconi, and D. Schofield 1978. Viking infrared thermal mapper. *Appl. Opt.* **17,** 1243–1251.

Conrath, B. J. 1981. Planetary-scale wave structure in the martian atmosphere. *Icarus* **48,** 246–255.

Ghil, M. M. Halem, and R. Atlas 1979. Time-continuous assimilation of remote-sounding data and its effect on weather forecasting. *Mon. Weather Rev.* **107,** 140–171.

Haberle, R. M., J. B. Pollack, J. R. Barnes, R. W. Zurek, C. B. Leovy, J. R. Murphy, H. Lee, and J. Schaeffer 1993. Mars atmospheric dynamics as simulated by the NASA Ames general circulation model. 1. The zonal mean circulation. *J. Geophys. Res.* **98,** 3093–3123.

Hamilton, K., and R. R. Garcia 1986. Theory and observation of the short-period normal mode oscillations of the atmosphere. *J. Geophys. Res.* **91,** 11,867–11,875.

Hollingsworth, J. L., and J. R. Barnes 1995. Forced, stationary planetary waves in Mars' winter atmosphere. *J. Atmos. Sci.,* submitted for publication.

Kahn, R. 1984. The spatial and seasonal distribution of martian clouds and some meteorological implications. *J. Geophys. Res.* **89,** 6671–6688.

Kieffer, H. H., P. R. Christensen, T. Z. Martin, E. D. Miner, and F. D. Palluconi 1976. Temperatures of the martian surface and atmosphere: Viking observations of diurnal and geometric variations. *Science* **194,** 1346–1351.

Krauss, W., R. Döscher, A. Lehmann, and T. Viehoff 1990. On eddy scales in the eastern and northern Atlantic ocean as a function of latitude. *J. Geophys. Res.* **95,** 18,049–18,056.

Martin, L. J., and R. W. Zurek 1993. An analysis of the history of dust activity on Mars. *J. Geophys. Res.* **98,** 3221–3246.

Martin, T. Z., and H. H. Kieffer 1979. Thermal infrared properties of the martian atmosphere. 2. The 15-μm band measurements. *J. Geophys. Res.* **84,** 2843–2852.

Murphy, J. R., C. B. Leovy, and J. E. Tillman 1990. Observations of martian surface winds at the Viking Lander 1 Site. *J. Geophys. Res.* **95,** 14,555–14,575.

Santee, M. L., and D. Crisp 1992. Thermal structure and dust loading of the martian atmosphere during late southern summer: Mariner 9 revisited. *J. Geophys. Res.* **98,** 3261–3279.

Seaman, R. S. 1977. Absolute and differential accuracy of analyses achievable with specified observational network characteristics. *Mon. Weather Rev.* **105,** 1211–1222.

Tillman, J. E., R. M. Henry, and S. L. Hess 1979. Frontal systems during passage of the martian north polar hood over the Viking Lander 2 site prior to the first 1977 dust storm. *J. Geophys. Res.* **84,** 2947–2955.